Composites Part B 217 (2021) 108915

Contents lists available at ScienceDirect

Composites Part B

journal homepage: www.elsevier.com/locate/compositesb

Reinforcement with intragranular dispersion of carbon nanotubes in aluminum matrix composites

Qibing Liu, Genlian Fan *, Zhanqiu Tan, Qiang Guo, Dingbang Xiong, Yishi Su, Zhiqiang Li **, Di Zhang

State Key Laboratory of Metal Matrix Composites, School of Material Science and Engineering, Shanghai Jiao Tong University, Shanghai, 200240, China

ARTICLE INFO

Keywords:
A. Metal-matrix composites (MMCs)
B. Mechanical properties
Intragranular dispersion
D. Microstructural analysis

ABSTRACT

Carbon nanotubes (CNTs) reinforced Al composites with a unique intragranular dispersion were obtained by using ultra-short CNTs. Nano-scaled CNTs were uniformly distributed inside the ultrafine Al grains. In comparison with typical CNT/Al composites with intergranular CNTs dispersion, this intragranular CNT/Al composites enable stronger dislocation pinning and retention, thereby exhibits simultaneous improvement in strength and ductility. The present intragranular dispersion strategy will provide inspirations for fabricating strong and ductile nanocarbon reinforced metal matrix composites.

1. Introduction

The boom of modern industry has brought new opportunities and challenges to the development of metal matrix composites which demonstrate unique mechanical properties including high specific elastic modulus, specific strength and wear resistance [1,2]. Especially, carbon nanotubes (CNTs) reinforced aluminum composites (CNT/Al), as a representative of metal matrix nanocomposites, have been brought to the forefront and extensively studied due to the desire for lighter and stronger structural materials in aerospace, automotive and transportation industries [3,4]. Many researches have been conducted on the preparation technology, microstructure and properties of CNT/Al composites [4–10]. Similar to other metal matrix composites, CNT/Al composites also possess improved strength, elastic modulus but low ductility, which becomes a bottleneck that hinders their applications. The weak interfacial bonding between CNTs and Al significantly deteriorates the strength and ductility and many studies have been done to improve the interfacial bonding [11–13]. However, the intrinsic reason is that along with the uniform dispersion of CNTs at grain boundaries, the grain size of the Al matrix is refined to ultra-fine grain (UFG) scale, which lacks of dislocation storage ability and leads to insufficient strain hardening rate [14–16]. To alleviate the dilemma of strength and ductility in Al composites, various architectural design strategies were proposed, such as nanolaminate architecture [9], alignment architecture [8] and bimodal architecture [17], which did improve the ductility to certain extent through the reduction of CNTs agglomeration, and/or introducing extrinsic toughening effect, or changing the grain configuration [4]. However, in all those architectural CNT/Al composites, *intergranular* distribution of CNTs can hardly trigger the intrinsic toughening mechanism.

It is generally accepted that for ultrafine grained metals, introduce *intragranular* nanoparticles would not only effectively improve strength, but would also benefit to ductility intrinsically by increasing the strain hardening ability [15,16,18,19]. Thus, intragranular dispersion of CNTs would be a promising pathway to further improve the strength and ductility in CNT/Al composites. However, intragranular CNTs are rarely reported in Al matrix composites. Recently, Kang's work shows that intragranular CNTs distribution in Al could be achieved by ball milling in the glove box environment to satisfy rigid no-oxidation condition [20]. However, inhibiting oxidation of Al is difficult during actual process because of the high activity of Al [21] and the factors affect intragranular CNTs still remain unclear.

We here demonstrate that by using ultra-short CNTs with dozens of nanometers, intragranular CNT/Al composites could be fabricated even in the presence of unavoidable oxygen. Ultra-short CNTs with length less than 100 nm were obtained by a novel short-cut treatment via a high-speed shearing process. Compared with the intergranular CNT/Al composites, the intragranular CNT/Al composites possess higher dislocation density and improved strain hardening rate, which significantly improves the yield strength and tensile ductility, while maintaining the

* Corresponding author.
** Corresponding author.
E-mail addresses: fangenlian@sjtu.edu.cn (G. Fan), lizhq@sjtu.edu.cn (Z. Li).

https://doi.org/10.1016/j.compositesb.2021.108915
Received 22 February 2021; Received in revised form 13 April 2021; Accepted 13 April 2021
Available online 18 April 2021
1359-8368/

high enhancement efficiency of Young's modulus.

2. Experimental

Graphitized CNTs (~15–30 nm in diameter and ~5–30 μm in length) and the atomized spherical pure Al powders (99.9% purity, ~20–40 μm in diameter) were chosen as raw materials. The fabrication of CNT/Al composites includes the high-speed shearing process for shortening CNTs and the flake powder metallurgy process for dispersing the CNTs and producing the composites.

2.1. Fabrication of ultra-short CNTs

To obtain ultra-short CNTs, ZrO_2 balls (80–120 μm in diameter) were mixed with CNTs and processed in a high-speed mechanical powder processor at 1500 rpm for 15 min, during which CNTs were shortened by the severe collision between ZrO_2 balls when passing through the small clearance (3 mm) between the blades and chamber wall [22,23], and then they were separated from the ZrO_2 balls by washing with alcohol and dried. The original CNTs and the CNTs treated by high-speed shearing process were named as Long CNTs and Short CNTs, respectively.

2.2. Flake powder metallurgy process to fabricate composites

0.5 wt.% Long and Short CNTs were mixed with Al powders and 1 wt. % stearic acid by shift-speed ball milling process in the stainless steel jar filled with Ar atmosphere [6], respectively, which includes low-speed ball milling (135 rpm for 6h) and high-speed ball milling (270 rpm for 1h). Degassing treatment were carried out at 375 °C for 3h between low and high-speed ball milling to remove stearic acid. Finally, the composites powders were compacted and sintered in a vacuum furnace (10^{-1} Pa) at 600 °C for 2h and extruded at 450 °C with an extrusion ratio of 25:1, as shown in Fig. 1. The composites reinforced with Long CNTs and Short CNTs were named as Long CNT/Al composites and Short CNT/Al composites, respectively.

2.3. Materials characterization

The microstructure of CNTs and CNT/Al composites was examined by a scanning transmission electron microscope (STEM, Talos F200X G2) operated at 200 kV. Focused ion beam milling (PIPS 695, Gatan) was used to prepare TEM samples of the composites. A SEM (MIRA 3, TESCAN) was used to characterize the evolution of CNTs and Al powders during ball milling. Raman spectroscopy tests were performed on SENTERRA R200-L with the 1064 nm line of an Ar+ laser as the excitation source, to identify the structural evolution of CNTs during fabrication. The grain size of materials was probed by electron backscattered diffraction (EBSD, NordlysMax3, Oxford) with a length step of 100 nm. The surface of EBSD samples was firstly grinded with 320–4000 grit metallographic silicon carbide papers, then polished in diamond suspensions, and finally ion polished (EM TIC 3X, Leica). The oxygen content of samples was measured by Oxygen–Nitrogen–Hydrogen Analyzer (EMGA-830, HORIBA Ltd.). The quasi-static tensile tests of plate samples with 8 mm gauge length and 1 mm thickness were conducted on a universal testing machine (Instron 3344) equipped with an automatic contacting extensometer at a constant strain rate of 5×10^{-4} s^{-1} at room temperature. The Young's modulus of composites was measured by resonance test at room temperature (Nihon-tech ET-RT) [24]. The length of CNTs in final composites was obtained by measurement from TEM images. The dislocation density evolution of composites during deformation was detected by X-ray diffraction with a Cu $K\alpha$ radiation source and estimated from the Williamson-Smallman relation [25]:

$$\rho = 2\sqrt{3} < \varepsilon^{1/2} > / d_{XRD} b \quad (1)$$

where $<\varepsilon^2>^{1/2}$ denotes the micro-strain, d_{XRD} the crystallite size and b the absolute value of Burgers vector for a full dislocation {111}<110> in fcc Al (b = 0.02862 nm).

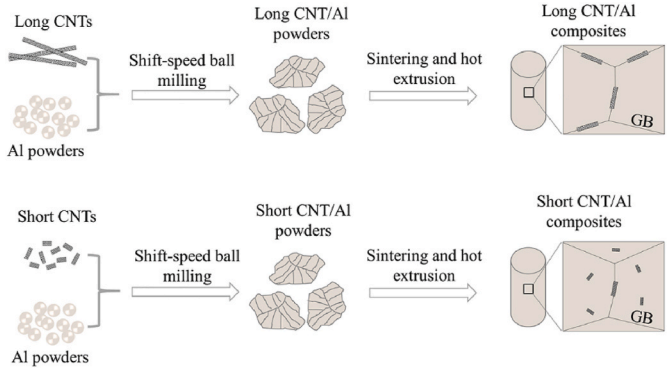

Fig. 1. Schematic diagram of fabrication of Long and Short CNT/Al composites via shift-speed ball milling, sintering and hot extrusion process.

3. Results

3.1. Microstructure evolution of Long and Short CNT/Al composites

Fig. 2a and b shows representative TEM micrograph of Long CNTs and Short CNTs. The initial length of Long CNTs was about 5–30 μm, and it was dramatically decreased to ~20–100 nm after high-speed shearing process. The insets show the corresponding HRTEM images, where the obscure outer layer of Short CNTs may result from the inevitable structural damage during the process. This is in agreement with the Raman spectra in Fig. 2e. The I_D/I_G value of Long CNTs was only 0.12 ± 0.02, while it increased to 1.01 ± 0.03 after short-cut treatment. During low-speed ball milling, the original spherical aluminum powders were deformed into nanoflakes and CNTs were dispersed uniformly on their surfaces as shown in Fig. 2c and d. It is worth noting that Long CNTs were also fractured during low-speed ball milling process, and the length decreased from 5-30 μm to about 150-500 nm, as shown in Fig. 2c. Raman spectra in Fig. 2e show that the I_D/I_G value of Long and Short CNT/Al composite powders after ball milling were 1.02 ± 0.11 and 1.04 ± 0.16, respectively, which indicated that the Long CNTs were also damaged during the ball milling process. The I_D/I_G value of the final Long CNT/Al and Short CNT/Al composites were also almost the same, to be 1.08 ± 0.09 and 1.09 ± 0.11, respectively. The peak for G-band of CNTs slightly shifted to higher wavelength after ball milling, which is related to the reduction in C–C distance by compression during ball milling and hot-extrusion [26]. The characteristic peaks of CNTs, D and G band, were clearly detected, and Al_4C_3 peaks were very weak. This indicates that most CNTs were well kept in both composites.

3.2. Microstructure of CNT/Al composites

3.2.1. Spatial distribution of CNTs in CNT/Al composites

Fig. 3a and b shows the TEM microstructure of Long and Short CNT/Al composites. In the Long CNT/Al composites, most CNTs were found located at grain boundaries, as shown in Fig. 3a. While in the Short CNT/Al composites, CNTs were mostly found inside the grains, as shown in Fig. 3b. Fig. 3c and d count the percentages of CNTs with different length ranges located in grain interiors or at grain boundaries, which were obtained based on TEM images. From the collected data, about 95% CNTs were located at grain boundaries in Long CNT/Al composites, in which the average length of CNTs is about 185 ± 54 nm. However, in Short CNT/Al composites with average CNTs length of 51 ± 25 nm, about 60% CNTs are located in grain interiors and 40% CNTs are located

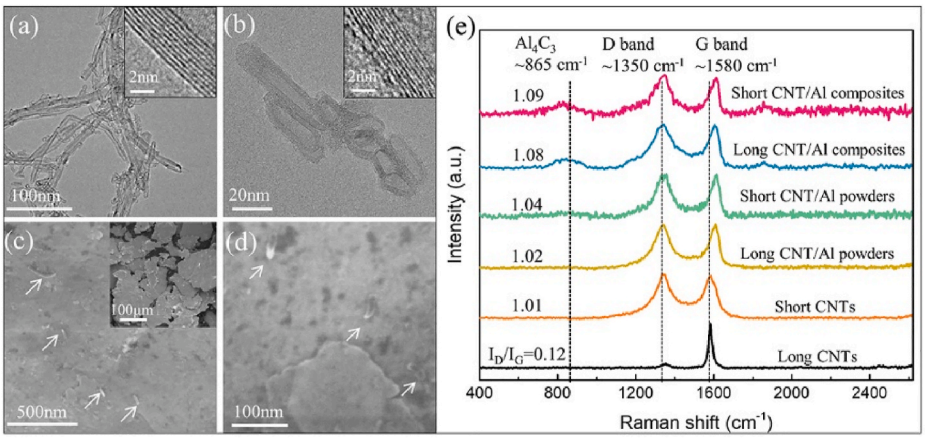

Fig. 2. TEM images of the (a) Long CNTs, (b) Short CNTs, with inset showing corresponding HRTEM. SEM images of (c) Long CNT/Al powders and (d) Short CNT/Al powders after low-speed ball milling, the inset shows Al nanoflakes, (e) Raman spectra of Long and Short CNTs and the corresponding CNT/Al composite powders and the extruded composites.

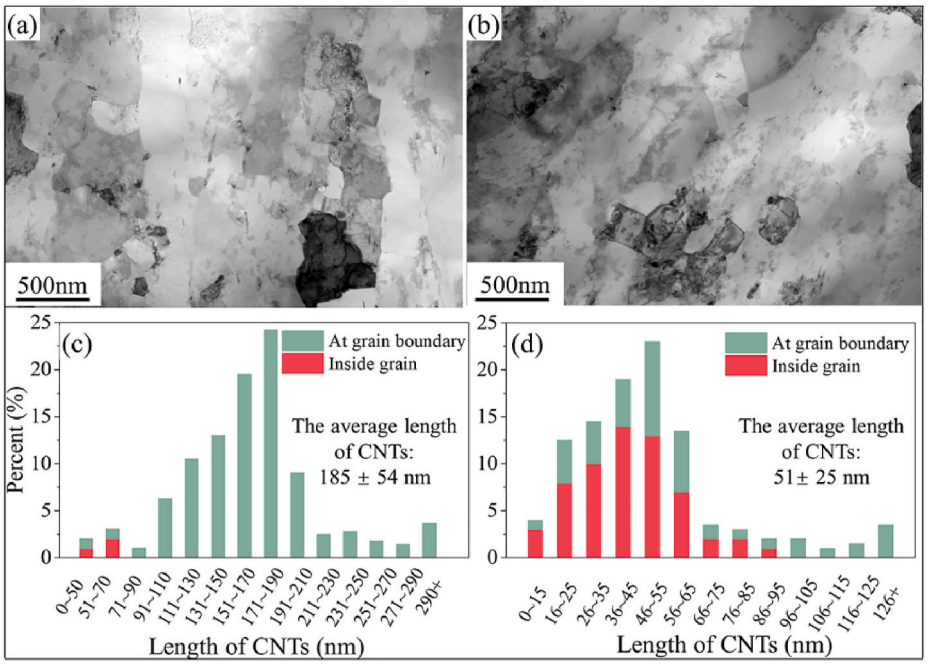

Fig. 3. TEM images of Long (a) and (b) Short CNT/Al composites. Percentage of intergranular and intragranular CNTs and their length distribution in extruded composites: (a) Long CNT/Al composites, (b) Short CNT/Al composites.

at grain boundaries. For those shorter than 95 nm, some of them are distributed in grain interiors and some are at grain boundaries. While those longer than 95 nm are only found at grain boundaries.

3.2.2. *Structure of CNTs in CNT/Al composites*

The distribution of CNTs in Long CNT/Al composites is shown in Fig. 4a, as marked with white arrows. Fig. 4b shows the HRTEM structure of CNTs, where a layer of γ-Al_2O_3 was found between CNTs and Al. Some γ-Al_2O_3 with low contrast were also detected inside grain interiors in Long CNT/Al composites, and the corresponding HRTEM is shown in Fig. 4c (the inset shows the FFT image). Some Al_4C_3 nanorods were detected in matrix and the HRTEM structure is shown in Fig. 4d.

The distribution of CNTs in Short CNT/Al composites is shown in Fig. 4e, as marked with white arrows. The HRTEM structure of CNTs located at grain boundary shows that a layer of γ-Al_2O_3 was found between CNTs and Al, which is similar with Long CNT/Al composites. Fig. 4g shows the HRTEM structure of intragranular CNTs, where the layer structure of CNTs is well remained. The γ-Al_2O_3 were sometimes found inside grain interior and the HRTEM structure was shown in Fig. 4h. The formation of γ-Al_2O_3 in samples is due to the high activity of Al, even purge ball milling jars with argon [21]. The γ-Al_2O_3 may be fractured and may encapsulate CNTs inside during the ball milling process because both CNTs and γ-Al_2O_3 are dispersed between Al nanoflakes. Besides, the interfacial energy between CNTs and Al is about 1.0 J/m^2 [27]. However, the interfacial energy of γ-Al_2O_3 and Al is about −2.254 J/m^2 [28]. Therefore, the inclusion of CNTs inside γ-Al_2O_3 is beneficial to decrease the thermodynamic energy, which may also lead to the formation of γ-Al_2O_3 on CNTs along grain boundaries in CNT/Al composites.

3.2.3. *EBSD images of Al, Long and Short CNT/Al composites*

Fig. 5 shows the EBSD images of Al, Long and Short CNT/Al composites. All the samples exhibited elongated grains. The average grain sizes of Al, Long and Short CNT/Al composites are about ~974 nm, 488

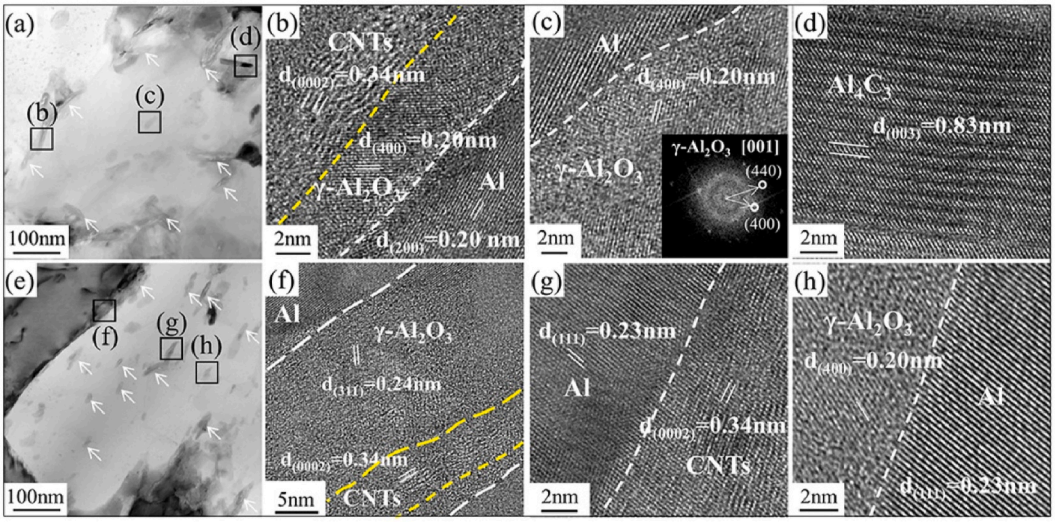

Fig. 4. STEM images of (a) Long CNT/Al composites, white arrows showing CNTs and (b–d) HRTEM showing structure of CNTs, γ-Al_2O_3 and Al_4C_3; (e) Short CNT/Al composites, white arrows showing CNTs, (f–h) HRTEM showing structure of the CNTs and γ-Al_2O_3.

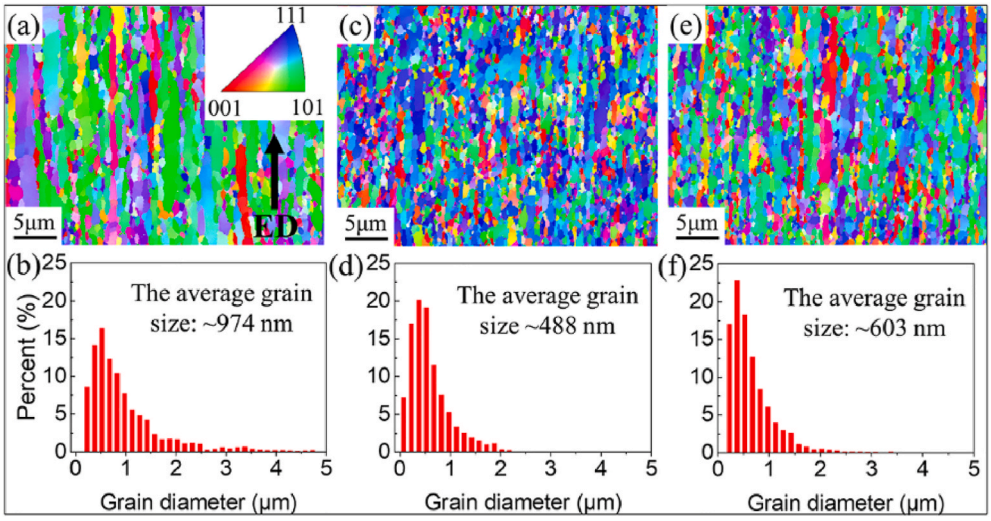

Fig. 5. EBSD images and corresponding grain size distribution: (a–b) Al, (c–d) Long CNT/Al composites, (e–f) Short CNT/Al composites.

nm and 603 nm, respectively. The smaller grain size of composites is due to the existence of CNTs, which pin the movement of grain boundary during recrystallization. In Short CNT/Al composites, the ultra-short CNTs introduce smaller Zener force upon grain boundary, resulting in significant grain growth comparing with Long CNT/Al composites. Therefore, the grain size of Short CNT/Al composites is relatively larger than that of Long CNT/Al composites.

3.3. Mechanical property of Al and CNT/Al composites

Fig. 6a and b shows the engineering tensile stress–strain curves and true stress-strain curves of Al and CNT/Al composites (the uniform elongation was marked by hollow dots), respectively, and the data were listed in Table 1. The Young's modulus of Al, Long and Short CNT/Al composites were ~75.4, ~79.7 and ~79.6 GPa, respectively.

The yield strength and tensile strength of Long CNT/Al composites were 204.1 ± 3.3 and 268.6 ± 2.4 MPa, which were ~11.8% and ~16.7% higher than those of Al (182.6 ± 3.1 and 230.0 ± 3.8 MPa), respectively. However, the elongation decreased from 14.2 ± 0.2% to 10.3 ± 0.3%. While the yield and tensile strength further increased to 232.2 ± 2.0 and 302.9 ± 3.1 MPa in the Short CNT/Al composites (~27.2% and ~31.7% enhancement over Al), respectively, but maintained similar elongation (14.1 ± 0.5%). These results indicate that intragranular CNTs are more effective in strengthening the Al matrix and more beneficial to retain ductility than intergranular CNTs. The corresponding curves of strain hardening rate ($\Theta = \partial\sigma/\partial\varepsilon$) are shown in Fig. 6c, where the Short CNT/Al composites possessed the highest strain hardening rate. The strengthening efficiency (R) of intragranular CNTs in this study was compared with various CNTs spatial distributions in Al (Fig. 6d). The R is defined by $(\sigma_c\text{-}\sigma_m)/w_f\sigma_m$, where σ_c denotes tensile strength of composites, σ_m the tensile strength of matrix, w_f the weight fraction of CNTs. Obviously, most intergranular CNTs including homogenous and lamellar structure increase reinforcement efficiency at some expenses of ductility. Comparing with intergranular CNTs, intragranular CNTs without oxygen possess better retention of elongation but insufficient reinforcement efficiency. However, the ultra-short intragranular CNTs in this study exhibit the highest reinforcement efficiency without sacrificing ductility.

To explore the source of the higher flow stress of the Short CNT/Al composites, the tensile loading-unloading testes at intervals of 0.5% nominal strain was carried out to study the Bauschinger effect [29–31]. The loading-unloading curves of Al, Long and Short CNT/Al composites

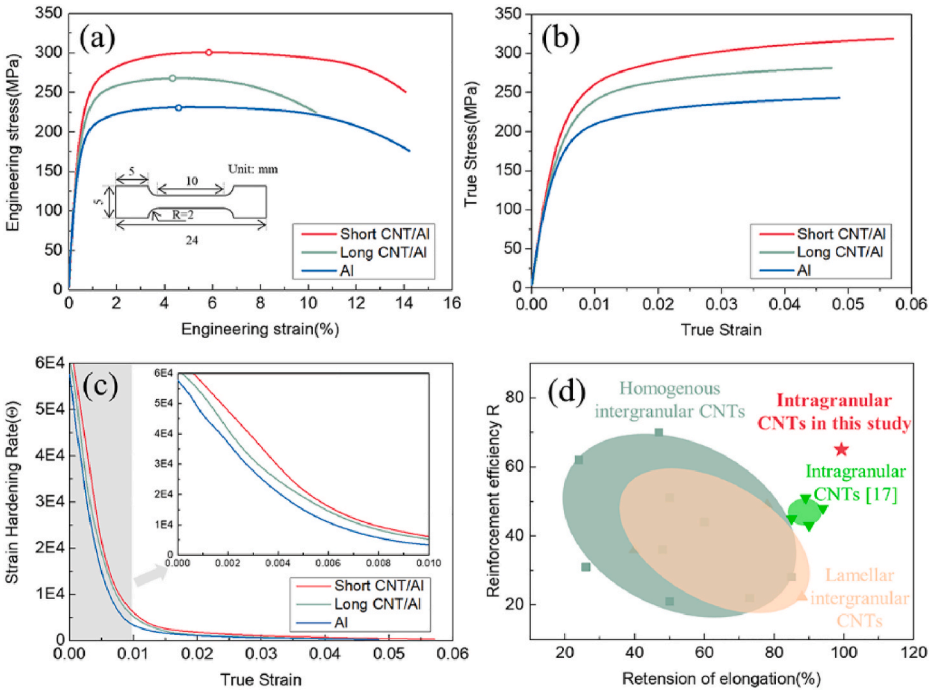

Fig. 6. (a) Engineering tensile stress–strain curves, (b) True stress-strain curves, (c) Strain hardening rate curves of Al, Long and Short CNT/Al composites. (d) Retention of fractural elongation versus strengthening efficiency, data was drawn based on review article [4] and ref. [17].

Table 1
Tensile properties of the Al, Long CNT/Al and Short CNT/Al composites.

Materials	Young's modulus (GPa)	Yield strength (MPa)	Ultimate tensile strength (MPa)	Total elongation (%)
Al	75.4 ± 0.8	182.6 ± 3.1	230.0 ± 2.8	14.2 ± 0.2
Long CNT/Al	79.7 ± 0.5	204.1 ± 3.3	268.6 ± 2.4	10.3 ± 0.3
Short CNT/Al	79.6 ± 0.6	232.2 ± 2.0	302.9 ± 3.1	14.1 ± 0.5

are shown in Fig. 7a. The effective stress and back stress of materials were calculated based on the methods in the study of Yang et al. [30]. As shown in Fig. 7b–d, compared with Al, the Long CNT/Al exhibited higher effective stress and back stress, which is due to the intergranular CNTs-induced geometrically necessary dislocations (GNDs) and long-range back stress [31]. Importantly, the effective stress and back stress in Short CNT/Al composites are higher than that of Long CNT/Al composites, resulting in the higher flow stress in Short CNT/Al composites.

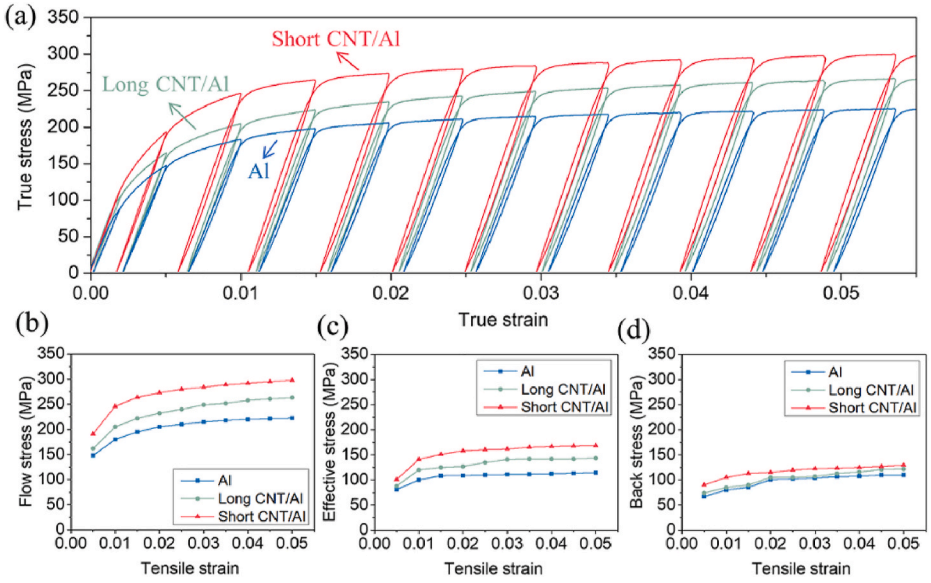

Fig. 7. (a) Loading-unloading curves of Al and CNT/Al composites; (b–d) flow stress, effective stress and back stress at different plastic strains of Al and CNT/Al composites.

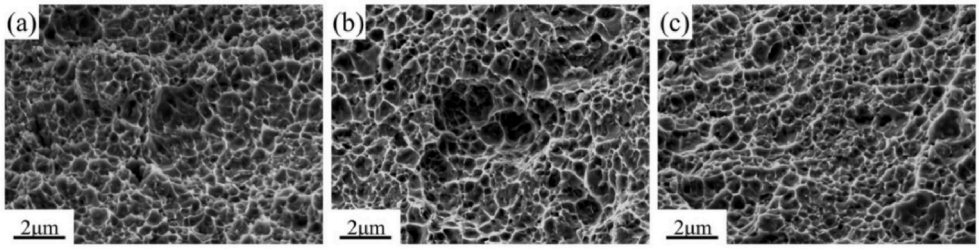

Fig. 8. Fracture morphology of (a) Al, (b) Long CNT/Al composites and (c) Short CNT/Al composites.

3.4. Fracture morphology of Al and CNT/Al composites

Fig. 8 shows the SEM images of fractured surface of Al, Long and Short CNT/Al composites. Both Al and composites exhibited typical ductile fracture surface consisted of dimples. However, in Long CNT/Al composites, large cave was observed, which was related to local early failure. In the Al and Short CNT/Al composites, the size of dimples was more uniform. This indicated that no obvious local early failure occurred in Al and Short CNT/Al composites.

3.5. Interaction of dislocations and CNTs in composites

Fig. 9a and b shows the STEM images of Long and Short composites after 4% tensile deformation (the sample for STEM observation of composites was cut from the middle of parallel zone of dog-bone specimen). In Long CNT/Al composites, dislocations were mainly hindered at the CNT/Al interface. In Short CNT/Al composites, dislocations were captured by intragranular CNTs before slipping to grain boundary. The corresponding evolution of dislocation density measured by XRD is shown in Fig. 9c and d. The dislocation densities of the as-extruded Long and Short CNT/Al composites were ~6.90 × 10^{13} m^{-2} and ~8.82 × 10^{13} m^{-2}, respectively. After 4% tensile deformation, the dislocation densities of the Long and Short CNT/Al composites increased to ~1.76 × 10^{14} m^{-2} and ~3.52 × 10^{14} m^{-2}, respectively, ~155% and ~300% enhancement over extruded state. The more dramatic increase of dislocation density in the Short CNT/Al composites confirmed that intragranular CNTs were more beneficial to dislocation accumulation in ultrafine grain matrix [15], leading to higher strain hardening rate (as shown in Fig. 6c) and enhancement of uniform elongation according to the Considére criterion [32].

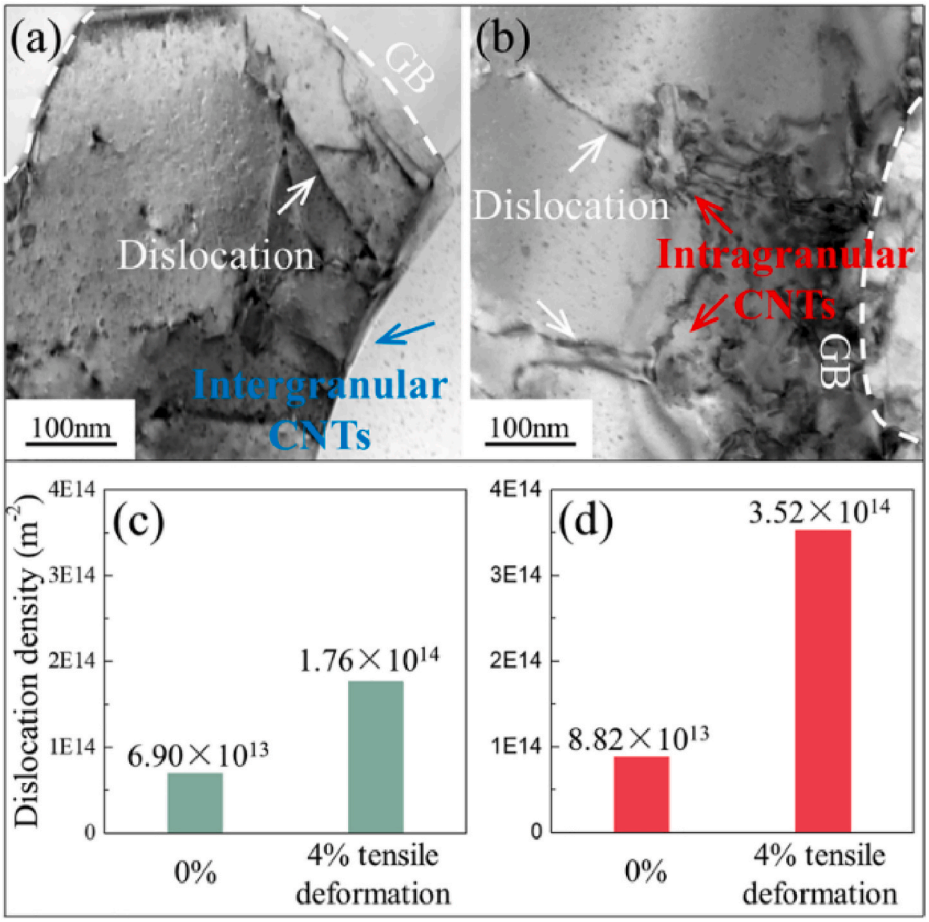

Fig. 9. STEM images and dislocation density of composites after 4% tensile deformation: (a), (c) Long CNT/Al composites and (b), (d)Short CNT/Al composites.

4. Discussions

4.1. The effect of CNTs length on their distribution

The formation of intragranular CNTs distribution in ultra-fine grain is accomplished by grain boundary (GB) migration and detachment of CNTs from GB [33]. When the driving force reaches the resistance Zener force, GB will detach from the particles and leave the particles inside the grains. The driving force mainly comes from the reduction of GB, which is independent of particles size [34]. However, the pinning force induced by particles is greatly affected by their size, which can be estimated by:

$$F_Z = 2\pi\gamma R_* cos\theta_* sin\theta \quad (2)$$

Where γ is the grain boundary energy, R is the particle size and θ is the angle between the GB line and the direction of GB motion [35]. Therefore, compared with Long CNTs, the ultra-short length of Short CNTs significantly reduces the Zener force, which is thermodynamically beneficial to the intragranular distribution.

Besides, particle size significantly influences the mobility kinetics of particles and GB. The mobility of particles can be expressed as:

$$m_p = \rho_s D_s \Omega^2/(\pi R^4 kT) \quad (3)$$

Where ρ_s denotes the surface density of atoms, D_s the surface diffusion constant, Ω the atomic volume, R the particle size, k the Boltzmann's constant and T the absolute temperature [36]. And the GB mobility is determined either by the particle mobility at low particle mobility or by the GB mobility at high particle mobility [36]. Thus, the large size of particles will dramatically decrease the mobility kinetics of particles, thereby reducing the mobility kinetics of GB. According to TEM observation in Fig. 3, the length of intragranular CNTs is generally less than 95 nm. Therefore, the critical length for the detachment of CNTs from GB at present deformation condition is estimated to be about 95 nm. Whereas the length of CNTs in the Long CNT/Al composites (185 ± 64 nm) was much longer than that of CNTs in Short CNT/Al composites, as shown in Fig. 3a, resulting in the inhibition of the detachment of CNTs from GB.

The results indicate that ultra-short length of CNTs is critical to achieve intragranular CNTs in Al matrix in this study. In Kang's work [20], it was supposed that the intragranular CNTs is accomplished by rapid surface diffusion of Al during ball milling. So, they suggest that no-oxidation condition is critical because oxygen layer will limit the diffusion-driven cold welding. Differently, in this study, intragranular CNTs are achieved by the interaction of CNTs and GB during the movement of GB in deformation process, which may be more suitable for practical process. Besides, the introducing of γ-Al_2O_3 is beneficial to protect CNTs from the formation of Al_4C_3 with Al.

4.2. Strengthening mechanisms induced by CNTs in composites

The main strengthening mechanisms in CNT/Al composites include thermal mismatch, grain refinement, load transfer and Orowan mechanism [21,37]. The thermal mismatch strengthening mechanism is related to the thermal expansion coefficients between CNTs and Al. Dislocations can be generated at the interface of CNTs and Al during fast cooling process. However, in this study, few dislocations were observed at the interface of CNTs and Al (Fig. 3), which might be due to the slow cooling rate after hot extrusion. Therefore, only three potential mechanisms, i.e., grain refinement, load transfer and Orowan to account for the strength improvement in CNT/Al composites. The yield strength of composites can be estimated by:

$$\sigma_c = \sigma_m + \Delta\sigma_{GR} + \Delta\sigma_{LT} + \Delta\sigma_{Orowan} \quad (4)$$

Where σ_m is the yield strength of Al.$\Delta\sigma_{GR}$, $\Delta\sigma_{LT}$ *and* $\Delta\sigma_{Orowan}$ are strengthening contribution from grain refinement, load transfer and Orowan strengthening mechanism, respectively.

4.2.1. Strengthening by grain refinement

The addition of CNTs to Al matrix can pin the movement of grain boundaries and refine the size of grains [6], and the corresponding strengthening can be calculated using the Hall-Petch mechanism by the following equation [38],

$$\Delta\sigma_{GR} = K(D_c^{-0.5} - D_m^{-0.5}) \quad (5)$$

where K is a constant (0.04 MPa $m^{0.5}$ for Al) [39], D_c and D_m are average grain diameter for composites and Al. The average grain sizes of Al, Long and Short CNT/Al composites were ~974 nm, ~488 and ~603 nm, respectively, as shown in Fig. 6. The calculated $\Delta\sigma_{H-P}$ of Long and Short CNT/Al composites in comparison with the Al were 16.7 and 11.0 MPa, respectively.

4.2.2. Strengthening by load transfer

The strengthening contribution by load transfer ($\Delta\sigma_{LT}$) can be estimated by the shear lag model [40] as:

$$\Delta\sigma_{LT} = 0.5V\sigma_m[Scos^2\theta + (\frac{3\pi-4}{3\pi})(1+\frac{1}{S})sin^2\theta] \quad (6)$$

Where V is the volume fraction of CNTs. V was taken as 0.75% for Long CNT/Al composites, however, V was 0.30% for Short CNT/Al composites (the intergranular CNTs in Short CNT/Al composites were ~40%). σ_m is the yield strength of Al matrix, which is about 180.6 MPa from experiment result. S is the aspect ratio of CNTs, where the S values of the Long and Short CNTs are 9.3 and 2.6 respectively. θ is the angle between CNTs and load direction (or extrusion direction of samples). During the extrusion process, the CNTs will be arranged in the direction of extrusion, but it is impossible for all the CNTs to be completely parallel to the direction of extrusion, so an intermediate value (45°) is taken. The calculated $\Delta\sigma_{LT}$ of Long and Short CNT/Al composites in comparison with the reference Al are 3.4 and 0.5 MPa, respectively.

4.2.3. Orowan strengthening

The strengthening effect caused by the intragranular CNTs is calculated by the Orowan mechanism [41]:

$$\Delta\sigma_{Orowan} = \frac{0.8MGb}{2\pi(1-\nu)^{1/2}}\frac{ln(d_p/b)}{(\lambda - d_p)} \quad (7)$$

Where M is the Taylor factor (3.06 for Al [42]), and G is the shear modulus (25.4 GPa for Al [43]), b is the Berber vector (0.286 nm), ν is Poisson's ratio 0.33, and λ is the average spacing of the reinforcements $\lambda = 0.5d_p(3\pi/2f_v)^{1/2}$ [44]. The f_v is volume fraction of intragranular CNTs. In Short CNT/Al composites, the volume fraction of total CNTs is 0.75%, including ~60% intragranular CNTs and ~40% intergranular CNTs. Due to the low aspect ratio of the Short CNTs, the size is estimated as a spherical model, so the diameter of the reinforcement $d_p = 31.3$ nm. The calculated $\Delta\sigma_{Orowan}$ of Short CNT/Al composites in comparison with the reference Al is 34.3 MPa.

The above calculation estimates the strengthening contribution from CNTs. Except the CNTs, the existence of Al_2O_3 also contribute to the strength, since Al oxidation would not be inhibited during powder metallurgy processing [21]. In this study, oxygen content in Al, Long and Short CNT/Al composites were measured to be ~1.28, 1.25 and 1.30. wt.%, respectively, that is about 2.0 vol% γ-Al_2O_3 by assuming that all the oxygen atoms are converted to γ-Al_2O_3. It is already known that Al_2O_3 will be fractured during high energy ball milling [45], and some of those distributed inside grain interior can improve strength by Orowan mechanism in CNT/Al composites [21,46]. We assume that the strength improvement from γ-Al_2O_3 is equal in all samples because of the same ball milling process and same content of γ-Al_2O_3.

As schematically shown in Fig. 10a, the calculated yield strength of

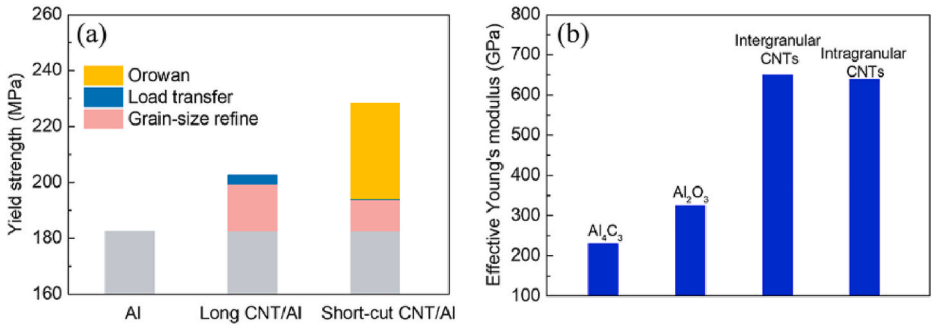

Fig. 10. (a) Calculated yield strength contribution related to intergranular and intragranular CNTs in composites; (b) Effective modulus of CNTs in this study and nanoparticles (the data was collected from Refs. [47,48]).

Long and Short CNT/Al composites based on equation (4) are 202.7 and 228.4 MPa, respectively, which reasonably agrees with experimental result (204.1 and 232.2 MPa). The above results indicate that when the reinforcements are moved from GB to grain interior, the dominated strengthening mechanism changes from grain refinement to Orowan.

4.2.4. The Young's modulus improvement by CNTs

It has been shown that the addition of CNTs in Al can improve the Young's modulus of matrix [4,24]. According to rule of mixture (ROM), the modulus of composites (*Em*) equals to Ref. [48]:

$$E_{Al}(1\text{-}V_{CNT}) + E_{CNTs}V_{CNTs} \tag{8}$$

Where E_{Al} is the modulus of Al, V_{CNT} is the volume fraction of CNTs and E_{CNTs} is the effective modulus of CNTs in this study. The modulus of Al and Short CNT/Al is 75.4 GPa and 79.6 GPa, respectively, and the volume fraction of CNTs is 0.75 vol%. According to equation (8), the effective modulus of CNTs can be inferred as 636 GPa in this study. The theoretical Young's modulus of CNTs is about 1 TPa [49], however, the structure damage is inevitably occurred during the fabrication process, leading to the effective modulus lower than the theoretical modulus of CNTs. Nevertheless, the effective modulus of intergranular and intragranular CNTs are still ~640 GPa and 630 GPa, respectively, which is much higher than the effective modulus of other nano reinforcements, such as Al_2O_3 (~325 GPa [47]) and Al_4C_3 (~230 GPa [48]), as shown in Fig. 10b.

4.3. The contribution of CNTs to flow stress in CNT/Al composites

In Long CNT/Al composites, most CNTs are located at grain boundary. The deformation incompatibility between the CNTs and the Al may cause the accumulation of strain gradients geometrically necessary dislocations (GNDs) [50]. The GNDs are constrained by the near-interface strain gradients during deformation, which provide back stress upon mobile dislocation [31]. resulting in higher flow stress than Al, as shown in Fig. 7. Differently, in Short CNT/Al composites, the shear-resistant intragranular CNTs could trap Orowan loops, which more effectively provides forest hardening and back stress hardening [51]. As a result, the higher effective stress and back stress induced by intragranular CNTs bring higher flow stress in Short CNT/Al composites comparing with Long CNT/Al composites, as shown in Fig. 7.

Besides, in Long CNT/Al composites, dislocations slip directly to grain boundary and generate stress concentration at the interface of CNTs, which may cause interface cracking. However, in Short CNT/Al composites, the slip of dislocation is firstly captured by intragranular CNTs, which may activate cross slip of dislocation [52,53]. Thus, the stress concentration at grain boundary is relieved in Short CNT/Al composites, which is beneficial to avoid the initiation of crack along grain boundary. Additionally, moving CNTs from boundary into grain interior can effectively reduce the defects generated by the agglomeration at grain boundaries, thereby being benefit to the retention of the plasticity [19,54].

5. Conclusion

In this study, we propose a high-speed shearing process to effectively fabricate ultra-short CNTs with dozens of nanometers. The strong and ductile CNT/Al with intragranular distribution is fabricated by using ultra-short CNTs and flake powder metallurgy. The following conclusions can be drawn from this study:

(1) The critical factor to achieve intragranular CNT/Al composites is ultra-short CNTs. Mostly CNTs were located at grain boundaries in Long CNT/Al composites with average CNTs length of 185 ± 54 nm. While about 60% CNTs (<95 nm) are located in grain interiors in Short CNT/Al composites with average CNTs length of 51 ± 25 nm.
(2) The intragranular CNT/Al composites possess the best combination of strength and ductility comparing with the intergranular ones. The 0.5 wt.% Short CNT/Al composites exhibited a yield strength, tensile strength and elongation of 232.2 ± 2.0 MPa, 302.9 ± 3.1 MPa and 14.1 ± 0.5%, respectively, which is about 13.7%, 12.8% and 36.7% higher than the Long CNT/Al composites.
(3) The spatial distribution of CNTs obviously influences the strengthening mechanisms in composites. In Long CNT/Al composites, the yield strength improvement mainly comes from grain refinement (~16.7 MPa) induced by intergranular CNTs. In Short CNT/Al composites, yield strength improvement mainly comes from Orowan strengthening (~34.3 MPa) related to intragranular CNTs, which is more effective to improve effective stress and back stress than intergranular CNTs in Long CNT/Al composites, leading to higher flow strength in Short CNT/Al composites.
(4) The Short CNT/Al composites exhibit highest hardening rate, comparing with Al and Long CNT/Al composites. This is due to the slip of dislocations is directly hindered by intragranular CNTs, which is beneficial to the accumulation of dislocation and higher density of dislocation, thus leading to the enhancement of uniform elongation in Short CNT/Al composites.
(5) The intragranular CNT/Al composites could be a promising structural material, since it has overwhelming advantage over the intergranular ones in strength and ductility, and higher enhancement efficiency in Young's modulus compared with other nanoparticles.

Author statement

Qibing Liu: Conceptualization, Investigation, Writing – original draft. Genlian Fan: Conceptualization, Supervision, Writing – review & editing. Zhanqiu Tan: Methodology. Qiang Guo: Formal analysis. Dingbang Xiong: Validation, Formal analysis. Yishi Su: Formal analysis.

Zhiqiang Li: Validation, Funding acquisition. Di Zhang: Supervision.

Declaration of competing interest

The authors declare that they have no known competing financial interests or personal relationships that could have appeared to influence the work reported in this paper.

Acknowledgements

This work was supported by the National Natural Science Foundation of China (Nos. 51871149, 51971206, 52011530034), Shanghai Science and Technology Committee (No. 19ZR1474900), and the Innovation Foundation of Shanghai Aerospace Science and Technology (No. SAST2018-064).

References

[1] Kaczmar J, Pietrzak K, Włosiński W. The production and application of metal matrix composite materials. J Mater Process Technol 2000;106(1–3):58–67.
[2] Miracle DJCs. Metal matrix composites–from science to technological significance. Compos Sci Technol 2005;65(15–16):2526–40.
[3] Tjong SC. Recent progress in the development and properties of novel metal matrix nanocomposites reinforced with carbon nanotubes and graphene nanosheets. Mater Sci Eng R Rep 2013;74(10):281–350.
[4] Zhang X, Zhao N, C.J.P.i.M.S. He. The superior mechanical and physical properties of nanocarbon reinforced bulk composites achieved by architecture design–a review. Prog Mater Sci 2020:100672.
[5] Esawi AM, Morsi K, Sayed A, Taher M, Lanka SJCS. Effect of carbon nanotube (CNT) content on the mechanical properties of CNT-reinforced aluminium composites. Compos Sci Technol 2010;70(16):2237–41.
[6] Xu R, Tan Z, Xiong D, Fan G, Guo Q, Zhang J, Su Y, Li Z, Zhang D. Balanced strength and ductility in CNT/Al composites achieved by flake powder metallurgy via shift-speed ball milling. Composites Part A 2017;96:57–66.
[7] Chen B, Kondoh K, Imai H, Umeda J, Takahashi M. Simultaneously enhancing strength and ductility of carbon nanotube/aluminum composites by improving bonding conditions. Scripta Mater 2016;113:158–62.
[8] Liu Z, Xiao B, Wang W, Ma ZJC. Developing high-performance aluminum matrix composites with directionally aligned carbon nanotubes by combining friction stir processing and subsequent rolling. Carbon 2013;62:35–42.
[9] Jiang L, Li Z, Fan G, Cao L, Zhang DJSM. Strong and ductile carbon nanotube/aluminum bulk nanolaminated composites with two-dimensional alignment of carbon nanotubes. Scripta Mater 2012;66(6):331–4.
[10] Jiang L, Li Z, Fan G, Cao L, Zhang D. The use of flake powder metallurgy to produce carbon nanotube (CNT)/aluminum composites with a homogenous CNT distribution. Carbon 2012;50(5):1993–8.
[11] Guo B, Song M, Zhang X, Liu Y, Cen X, Chen B, Li W. Exploiting the synergic strengthening effects of stacking faults in carbon nanotubes reinforced aluminum matrix composites for enhanced mechanical properties. Compos B Eng 2021;211:108646.
[12] Guo B, Zhang X, Cen X, Chen B, Wang X, Song M, Ni S, Yi J, Shen T, Du Y. Enhanced mechanical properties of aluminum based composites reinforced by chemically oxidized carbon nanotubes. Carbon 2018;139:459–71.
[13] Guo B, Chen Y, Wang Z, Yi J, Ni S, Du Y, Li W, Song MJC. Enhancement of strength and ductility by interfacial nano-decoration in carbon nanotube/aluminum matrix composites. Carbon 2020;159:201–12.
[14] Ma E. Instabilities and ductility of nanocrystalline and ultrafine-grained metals. Scripta Mater 2003;49(7):663–8.
[15] Ma E. Eight routes to improve the tensile ductility of bulk nanostructured metals and alloys. J Occup Med 2006;58(4):49–53.
[16] Ovid'Ko I, Valiev R, Zhu Y. Review on superior strength and enhanced ductility of metallic nanomaterials. Prog Mater Sci 2018;94:462–540.
[17] Salama EI, Abbas A, A.M.J.C.P.A.A.S. Esawi. Manufacturing, Preparation and properties of dual-matrix carbon nanotube-reinforced aluminum composites. Composites Part A 2017;99:84–93.
[18] Liu G, Zhang G, Jiang F, Ding X, Sun Y, Sun J, Ma EJNm. Nanostructured high-strength molybdenum alloys with unprecedented tensile ductility. Nat Mater 2013;12(4):344–50.
[19] Hu C, Lai C, Du X, Ho N, Huang J. Enhanced tensile plasticity in ultrafine-grained metallic composite fabricated by friction stir process. Scripta Mater 2008;59(11):1163–6.
[20] So KP, Kushima A, Park JG, Liu X, Keum DH, Jeong HY, Yao F, Joo SH, Kim HS, Kim HJAS. Intragranular dispersion of carbon nanotubes comprehensively improves aluminum alloys. Adv Sci 2018;5(7):1800115.
[21] Chen B, Shen J, Ye X, Jia L, Li S, Umeda J, Takahashi M, Kondoh K. Length effect of carbon nanotubes on the strengthening mechanisms in metal matrix composites. Acta Mater 2017;140:317–25.
[22] Chen M, Fan G, Tan Z, Xiong D, Guo Q, Su Y, Zhang J, Li Z, Naito M, Zhang D. Design of an efficient flake powder metallurgy route to fabricate CNT/6061Al composites. Mater Des 2018;142:288–96.
[23] Chen M, Fan G, Tan Z, Yuan C, Xiong D, Guo Q, Su Y, Naito M, Li Z. Tailoring and characterization of carbon nanotube dispersity in CNT/6061Al composites. Mater Sci Eng, A 2019;757:172–81.
[24] Yu Z-Y, Tan Z-Q, Fan G-L, Lin R-B, Xiong D-B, Guo Q, Su Y-S, Li Z-Q, Zhang DJAMS. Young's modulus enhancement and measurement in CNT/Al nanocomposites. Acta Metall Sin (Engl Lett) 2018;31(11):1121–9.
[25] Williamson G, Smallman III RJPM. Dislocation densities in some annealed and cold-worked metals from measurements on the X-ray debye-scherrer spectrum. Philos Mag 1956;1(1):34–46.
[26] Schadler L, Giannaris Sa, Ajayan PJApl. Load transfer in carbon nanotube epoxy composites. Appl Phys Lett 1998;73(26):3842–4.
[27] Laha T, Kuchibhatla S, Seal S, Li W, Agarwal AJAM. Interfacial phenomena in thermally sprayed multiwalled carbon nanotube reinforced aluminum nanocomposite. Acta Mater 2007;55(3):1059–66.
[28] Jeurgens L, Sloof W, Tichelaar F, Mittemeijer EJPRB. Thermodynamic stability of amorphous oxide films on metals: application to aluminum oxide films on aluminum substrates. Phys Rev B 2000;62(7):4707.
[29] Kiser M, Zok F, Wilkinson DJAm. Plastic flow and fracture of a particulate metal matrix composite. Acta Mater 1996;44(9):3465–76.
[30] Yang M, Pan Y, Yuan F, Zhu Y, Wu XJMRL. Back stress strengthening and strain hardening in gradient structure. Mater. Res. Lett. 2016;4(3):145–51.
[31] Xu R, Fan G, Tan Z, Ji G, Chen C, Beausir B, Xiong D-B, Guo Q, Guo C, Li Z. Back stress in strain hardening of carbon nanotube/aluminum composites. Mater. Res. Lett. 2018;6(2):113–20.
[32] Dieter GE, Bacon DJ. Mechanical metallurgy. New York: McGraw-hill; 1986.
[33] Gottstein G, Shvindlerman LS. Grain boundary migration in metals: thermodynamics, kinetics, applications. CRC press; 2009.
[34] Huang K, Logé RJM. Design, A review of dynamic recrystallization phenomena in metallic materials. Mater Des 2016;111:548–74.
[35] Nes E, Ryum N, Hunderi OJAM. On the Zener drag. Acta Metall 1985;33(1):11–22.
[36] Gottstein G, Shvindlerman LS. Theory of grain boundary motion in the presence of mobile particles. Acta Mater 1993;41(11):3267–75.
[37] Chen B, Li S, Imai H, Jia L, Umeda J, Takahashi M, Kondoh KJCS. Technology, Load transfer strengthening in carbon nanotubes reinforced metal matrix composites via in-situ tensile tests. Compos Sci Technol 2015;113:1–8.
[38] Hansen NJSM. Hall–Petch relation and boundary strengthening. Scripta Mater 2004;51(8):801–6.
[39] Nam DH, Cha SI, Lim BK, Park HM, Han DS, Hong SHJC. Synergistic strengthening by load transfer mechanism and grain refinement of CNT/Al–Cu composites. Carbon 2012;50(7):2417–23.
[40] Ryu HJ, Cha SI, S.H.J.J.o.m.r. Hong. Generalized shear-lag model for load transfer in SiC/Al metal-matrix composites. J Mater Res 2003;18(12):2851–8.
[41] Aikin Jr R, L.J.S.M.e.M. Christodoulou. The role of equiaxed particles on the yield stress of composites. Scripta Metall Mater 1991;25(1):9–14.
[42] Stoller R, S.J.J.o.N.M. Zinkle. On the relationship between uniaxial yield strength and resolved shear stress in polycrystalline materials. J Nucl Mater 2000;283:349–52.
[43] Totten GE, MacKenzie DS. Handbook of aluminum: vol. 1: physical metallurgy and processes. CRC press; 2003.
[44] Le Roy G, Embury J, Edwards G, Ashby MJAM. A model of ductile fracture based on the nucleation and growth of voids. Acta Metall 1981;29(8):1509–22.
[45] Fan G, Jiang Y, Tan Z, Guo Q, Xiong D-b, Su Y, Lin R, Hu L, Li Z, Zhang DJC. Enhanced interfacial bonding and mechanical properties in CNT/Al composites fabricated by flake powder metallurgy. Carbon 2018;130:333–9.
[46] Chen B, Kondoh K, Li J, M.J.C.P.B.E. Qian. Extraordinary reinforcing effect of carbon nanotubes in aluminium matrix composites assisted by in-situ alumina nanoparticles. Composites Part B 2020;183:107691.
[47] Suryanarayana C. Synthesis of nanocomposites by mechanical alloying. J Alloys Compd 2011;509:S229–34.
[48] Yu Z, Tan Z, Fan G, Xiong D-B, Guo Q, Lin R, Hu L, Li Z, Zhang DJMC. Effect of interfacial reaction on Young's modulus in CNT/Al nanocomposite: a quantitative analysis. Mater Char 2018;137:84–90.
[49] Salvetat J-P, Briggs GAD, Bonard J-M, Bacsa RR, Kulik AJ, Stöckli T, Burnham NA, Forró LJPrl. Elastic and shear moduli of single-walled carbon nanotube ropes. Phys Rev Lett 1999;82(5):944.
[50] Ashby MF. The deformation of plastically non-homogeneous materials. Phil Mag: A Journal of Theoretical Experimental and Applied Physics 1970;21(170):399–424.
[51] da Costa Teixeira J, Bourgeois L, Sinclair CW, Hutchinson CRJAm. The effect of shear-resistant, plate-shaped precipitates on the work hardening of Al alloys: towards a prediction of the strength–elongation correlation. Acta Mater 2009;57(20):6075–89.
[52] Xiang Y, Srolovitz DJPm. Dislocation climb effects on particle bypass mechanisms. Philos Mag 2006;86(25–26):3937–57.
[53] MacEwen S, Hirsch P, , V.J.T.P.M.A.J.o.T.E. Vitek, Physics A. Cross-slip of Orowan loops at incoherent particles. Philos Mag 1973;28(3):703–23.
[54] Li A, Wang G, Zhang X, Li Y, Gao X, Sun H, Qian M, Cui X, Geng L, Fan G. Enhanced combination of strength and ductility in ultrafine-grained aluminum composites reinforced with high content intragranular nanoparticles. Mater Sci Eng, A 2019;745:10–9.